Article ID: 1000-324X(2020)03-0293-08 **DOI:** 10.15541/jim20190381

Microscopic Insights into pH-dependent Adsorption of Cd(II) on Molybdenum Disulfide Nanosheets

DONG Lijia[1], GUO Xiaojie[2], LI Xue[1], CHEN Chaogui[1], JIN Yang[1], AHMED Alsaedi[3], TASAWAR Hayat[3,4], ZHAO Qingzhou[5], SHENG Guodong[6]

(1. School of Life Science, Shaoxing University, Shaoxing 312000, China; 2. College of Materials & Environmental Engineering, Hangzhou Dianzi University, Hangzhou 310018, China; 3. NAAM Research Group, Department of Mathematics, Faculty of Science, King Abdulaziz University, Jeddah 21589, Saudi Arabia; 4. Department of Mathematics, Quaid-I-Azam University, Islamabad 44000, Pakistan; 5. College of Resources and Environment, University of Chinese Academy of Sciences, Beijing 100049, China; 6. College of Chemistry and Chemical Engineering, Shaoxing Univeristry, Shaoxing 312000, China)

Abstract: Herein, the retention mechanisms and microstructure of Cd(II) on MoS_2 nanosheets were evaluated by batch experiments and EXAFS technology. The sorption of Cd(II) on MoS_2 was strongly affected by solution pH, contact time, and temperature, but not by the ionic strength. The solution pH could only promote the sorption capacity, but does not improve the sorption rates and change the sorption isotherms and thermodynamics in the pH range of 3.3–9.6. The pseudo-second-order model could fit the equilibrium data better and the intra-particle diffusion model showed three typical stages in the sorption process. The isotherms and thermodynamics analysis indicated that the heterogeneity sorption of Cd(II) onto MoS_2 was a spontaneous, endothermic, and irreversible process. The EXAFS spectra revealed the coexistence of two sorption types. The inner-sphere complexation was formed in the form of Cd–S bond at lower pH (3.56, 6.48), while the $Cd(OH)_2$ precipitation occurred in the form of Cd–O and Cd–Cd bonds at higher pH (9.57). These results provide new insights into the interaction mechanisms between metal ions and MoS_2 nanosheets.

Key words: MoS_2 nanosheets; pH; microstructure; EXAFS; cadmium(II)

Cadmium (Cd(II)) is one of the toxic heavy metals from industrial activity such as nickel-cadmium batteries, mining, paint pigmentations, alloy, and electroplating[1-2]. With the input flux increasing, the Cd pollution is posing a great pressure on environmental safety[3]. Especially for the human public health, Cd(II) is very nasty due to its long biological half-life, non-biodegradable nature, and carcinogenicity[4-5]. Then appropriate removal technologies become necessary. Adsorption is considered as one of the promising techniques owing to its low cost, reliability, simplicity and high efficiency[6-9]. Since the adsorption reaction, mobility and species of metal ions in the environment determined their fate[10-16], it is of great importance to explore the interaction mechanism and microstructure of heavy metals at the solid/water interface in various environmental conditions.

Molybdenum disulfide (MoS_2), a "rising star" material, has attracted tremendous interest in remediation of heavy metals from water over past decades[17-20]. MoS_2 nanosheets have layered structure with strong in-plane bonding in layers and weak out-of-plane van der Waals interactions between the individual sandwiched S-Mo-S layers[21-23]. Based on the anisotropic structure of MoS_2, two-dimensional (2D) structure with large surface area and permeable channels for ion adsorption and transportation is prone to form[23]. It is noted that both surfaces of each layer of MoS_2 are fully occupied by S atoms, which may serve as binding sites [19-21]. In addition, MoS_2 offers some excellent properties like superior mechanical flexibility, excellent chemical and thermal stability. All above properties endow MoS_2 nanosheets with good adsorption performance for the removal of heavy metals. In several cases, the maximum sorption capacities of MoS_2 nanosheets for Hg(II), Ag(I), U(VI), Cd(II),

Received date: 2019-07-24; **Revised date:** 2019-09-11
Foundation item: National Natural Science Foundation of China (31700476)
Biography: DONG Lijia(1984–), female, PhD. E-mail: Donglijia@126.com
董丽佳(1984–), 女, 博士. E-mail: Donglijia@126.com
Corresponding author: JIN Yang, professor. E-mail: jyk@usx.edu.cn; SHENG Guodong, PhD. E-mail: gdsheng@usx.edu.cn.
金 阳, 教授级高级工程师. E-mail: jyk@usx.edu.cn; 盛国栋, 博士. E-mail: gdsheng@usx.edu.cn.

Th(IV) are up to 2506, 1348, 493, 477, 454 mg/g, respectively[21,24-26].

Many mechanisms have been proposed for the interaction of metals with MoS_2, including ion exchange, inner layer metal-S complexation, outer layer electrostatic attraction, surface precipitation[25-28]. Extended X-ray adsorption fine structure (EXAFS) spectroscopy provides an effective way to distinguish the interaction mechanism and microstructure[29]. In the past, the EXAFS technology was widely applied to reveal the interaction mechanisms and microstructures of heavy metals and adsorbents, such as Eu(III) and γ-MnOOH, Eu(III) and δ-MnO_2, Cd(II) and kaolinite, and Cd(II) and HAs[29-33]. However, few studies[34-36] about the interaction mechanism of heavy metals and MoS_2 nanosheets have been conducted at the molecular level.

In present work, both batch experiment and EXAFS technique were employed to analyze the sorption behavior and mechanism of Cd(II) on MoS_2. Firstly, MoS_2 were characterized by SEM, TEM, XRD, FT-IR, *etc*. Secondly, effects of solution pH, ionic strength, and temperature, contact time on the sorption of Cd(II) and the adsorption kinetics, isotherms, thermodynamics in solutions with various pH were evaluated. Finally, EXAFS technique was used to analyze the sorption mechanisms of Cd(II) on MoS_2 as a function of pH.

1 Materials and methods

1.1 Materials

Overall chemical reagents including cadmium nitrate ($Cd(NO_3)_2{\cdot}2H_2O$), sodium nitrate ($NaNO_3$), sodium hydroxide (NaOH), nitrite acid (HNO_3), and molybdenum disulfide (MoS_2) were analytical grade purchased from Nanjing XFNANO Materials Tech. Co. Ltd. (China) without further purification. Cd(II) stock solution was obtained by dissolving $Cd(NO_3)_2{\cdot}2H_2O$ in distilled water.

1.2 Characterization

The intrinsic properties of MoS_2 greatly determinate its sorption capacity, thereby it is helpful to investigate its characterization for revealing the sorption mechanism. Herein, TEM, SEM, EDX analysis and elemental distribution mappings of the MoS_2 sample were carried out by using a transmission electron microscope (JEM-1011, Japan) instrument and a field emission scanning electron microscope (JSM-6360LV, Japan). XRD pattern of the sample was tested by the D8 Discover X-ray diffractometer (Bruker, Germany) with Cu K_α radiation (λ=0.1541 nm) and distinguished according to the JCPD standards. FT-IR spectrometer (NEXUS, America) was employed to evaluate surface functional groups of MoS_2 in the wavelength range of 400–4000 cm^{-1}. Zeta potential analyzer (Zetasizer Nano ZS, Malvern Co., UK) was used to locate the pH_{pzc} of the adsorbent, *i.e.*, the suspension of MoS_2 and $NaNO_3$ adjusted to an appropriate pH was test.

1.3 Batch experiment

A set of sorption experiments of Cd(II) onto MoS_2 were conducted under N_2 in polyethylene tubes. The stock suspensions of Cd(II), MoS_2, $NaNO_3$, and distilled water were mixed in polyethylene tubes in order to gain the desired concentrations. The pH was adjusted by adding 0.1 or 0.01 mol/L HNO_3 or NaOH solution with negligible volumes. The tubes containing above mentioned mixtures were shaken for more than 12 h to achieve sorption equilibrium, and the the solid was separated by centrifugation method. Finally, the Cd concentration in the supernatant was tested. The Cd(II) sorption percentage, distribution coefficient (K_d), and sorption amount (q_e) on MoS_2 were calculated based on the following equations:

$$\text{Sorption\%}=(C_0-C_e)/C_0\times100\% \quad (1)$$

$$K_d=(C_0-C_e)/C_e\times V/m \quad (2)$$

$$q_e=(C_0-C_e)\times V/m \quad (3)$$

where C_0 and C_e represent the initial and equilibrium concentrations of Cd(II) (mg/L), respectively. V is the suspension volume (L) and m is the MoS_2 mass (g).

1.4 EXAFS data collection and analysis

EXAFS data were collected at room temperature on BL14W at Shanghai Synchrotron Radiation Facility (SSRF, China). The obtained EXAFS data was analyzed by using Athnea software. The raw, averaged data were processed to isolate the EXAFS oscillations by removal of the pre-edge background. The k^3-weighted EXAFS spectra of Cd(II) were Fourier transformed (FT). The code FEEF7 and the as-known crystal structure of $Cd(NO_3)_2$, $Cd(OH)_2$, CdS were used to calculate the theoretical scattering phases and amplitudes. The bond distance (R) and coordination number (CN), and the Debye-Waller factor of sample were optimized for each single peak by performing curve fitting with nonlinear least-squares.

2 Results and discussion

2.1 Characterization of MoS_2 nanosheets

The morphologies and microstructures of MoS_2 were characterized by SEM, TEM, *etc.*, and the results are shown in Fig. S1 in detail. SEM images, EDX spectra, and elemental distribution mapping of MoS_2 are shown in Fig. 1. It is evident that two non-target elements are present in MoS_2 nanosheets, *i.e.*, Cu and Zn. However, the elemental distribution percentages of Mo and S atoms are much higher than those of Cu and Zn, indicating that MoS_2 contains negligible impurities. In other words, the effects of Cu and Zn in MoS_2 materials on sorption can be ignored.

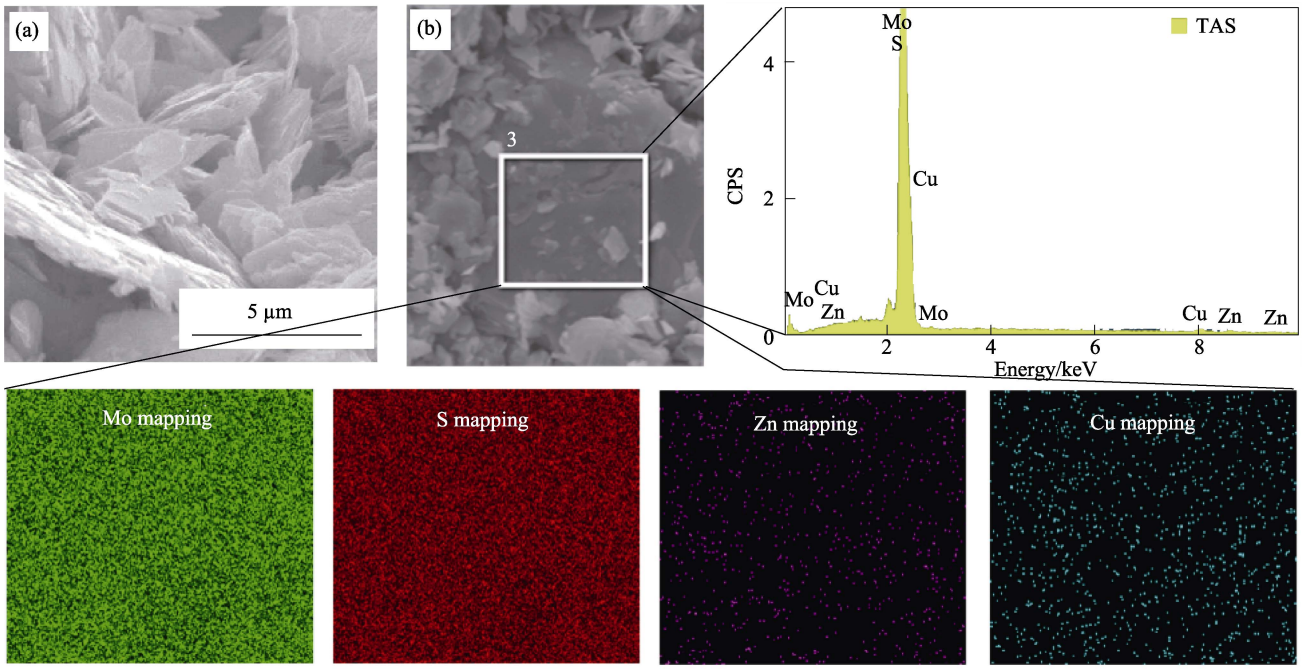

Fig. 1　SEM image (a), EDX spectra, and corresponding elemental maps (b) for MoS_2 nanosheets

2.2　Batch sorption

Fig. 2 shows the pH dependence of Cd(II) sorption on MoS_2 in 0.1, 0.01 and 0.001 mol/L $NaNO_3$ solutions, respectively. It is observed that the sorption is strongly dependent on pH. The percentage of Cd(II) sorption sharply increased at pH 3.3–6.5 and then creeped until a plateau level at pH>6.5. At pH 3.3–6.5, owing to protonation reaction, the number of protonated sites decreased with the increase of pH, leading to stronger affinity between the ions and MoS_2. However, the saturated surface of MoS_2 immobilized more cadmium ions at pH>6.5. It is noted that the species of Cd(II) are highly dependent on the solution pH. As provided by Wang *et al.*[25], the main species were Cd^{2+}, $CdOH^+$ at pH<8.5, whereas the main species were $Cd(OH)_2$ and $Cd(OH)^-$ at pH>8.5. Therefore, both electrostatic interaction and precipitation might be the main mechanisms of the sorption.

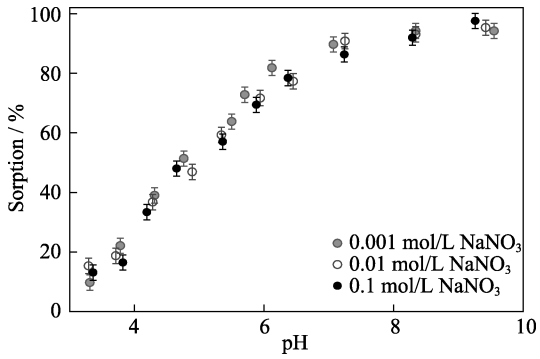

Fig. 2　Effects of pH and ionic strength on Cd(II) adsoprtion onto MoS_2 nanosheets

Cd(II) initial concentration=10 mg/L, m/V=0.15 g/L, T=293 K

Ionic strength is another important factor influencing sorption. Fig. 2 shows that the effect of ionic strength on Cd(II) sorption is not significant, implying inner-sphere complexation dominates the sorption behavior at different pH. The complexation type of Cd(II) with MoS_2 is different from that with other materials, such as montmorillonite[37], kaolinite[31], manganese oxide[38], fibre fruit lufa[39], magnetic polyvinyl alcohol/ laponite[40]. The interactions between Cd(II) and these materials were found to contain both outer-sphere complexation at lower pH and inner-sphere complexation at higher pH. The difference may be attributed to various microstructure and intrinsic properties among these adsorbents.

To understand the sorption kinetics and to determine their phenomenological coefficients, the sorption capacity as a function of contact time was shown in Fig. 3(a). The sorption rates at different pH were similar and the contact time needed for complete adsorption of Cd(II) on MoS_2 was 2 h. The final sorption capacities at pH 4.55, 5.34, and 6.12 reached 28.4, 37.2 and 49.3 mg/g, respectively. These results illustrate that pH only enhances the sorption capacity but does not promote the sorption rate. Besides, 3 kinetic models were employed to analyze the kinetic data, including pseudo-first- kinetic model[41], pseudo-second-kinetic model[42], and intra-particle diffusion model[43], which was described by follows:

$$\lg(q_e - q_t) = \lg q_e - k_1 t / 2.303 \quad (4)$$

$$\frac{t}{q_t} = \frac{1}{2k_2 q_e^2} + \frac{t}{q_e} \quad (5)$$

$$q_t = k_i t + C \quad (6)$$

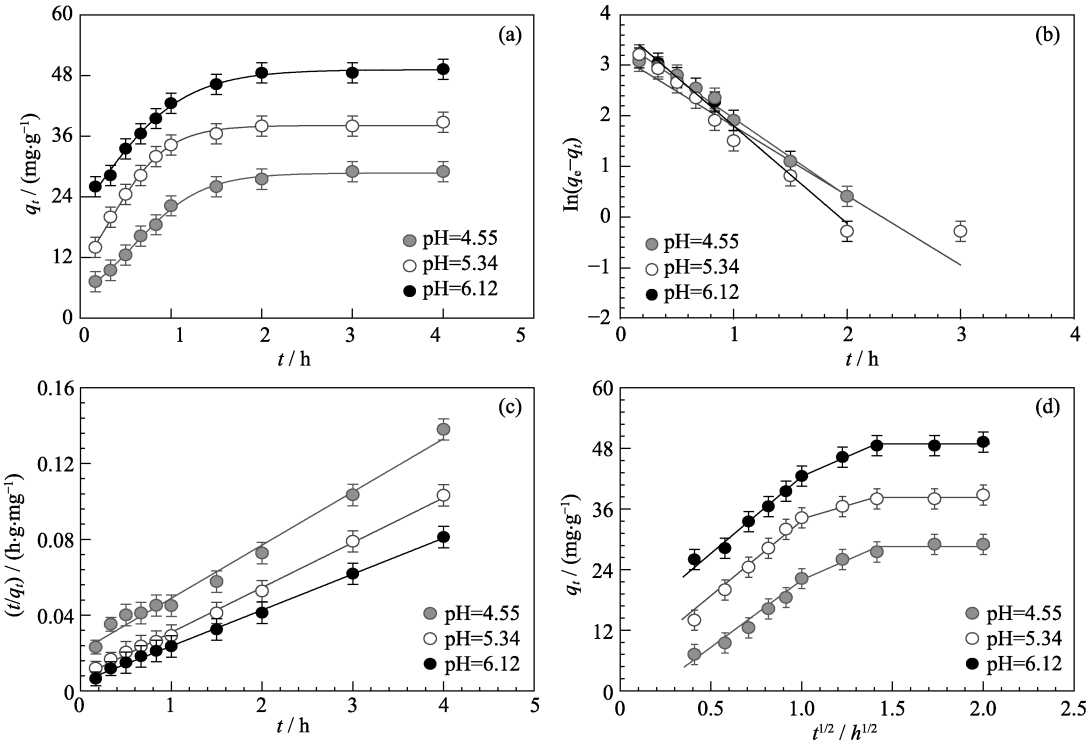

Fig. 3 Cd(II) adsorption on MoS_2 nanosheets as a function of contact time (a) and the fitting of pseudo-first-order kinetic model (b), pseudo-second-order kinetic model (c) and intra-particle diffusion model (d) at different pH

Cd(II) initial concentration=10 mg/L, m/V=0.15 g/L, I=0.01 mol/L $NaNO_3$, T=293 K

Table 1 Parameters of kinetic models for the adsorption of Cd(II) on MoS_2 as a function of pH

	pH	q_e/(mg·g^{-1})	k_1/h^{-1}	R^2
Pseudo-first-order model	4.55	33.023	0.059	0.9896
	5.34	23.903	0.053	0.9069
	6.12	41.777	0.074	0.9835
	pH	q_e/(mg·g^{-1})	k_2/(g·mg^{-1}·h^{-1})	R^2
Pseudo-second-order model	4.55	35.638	0.038	0.9869
	5.34	42.230	0.078	0.9978
	6.12	52.659	0.077	0.9986
	pH	C/(mg·L^{-1})	k_i/(g·mg^{-1}·h$^{-1/2}$)	R^2
Intra-particle diffusion model	4.55	19.985	2.628	0.942
	5.34	32.500	1.877	0.987
	6.12	39.759	3.004	0.980

Cd(II) initial concentration=10 mg/L, m/V=0.15 g/L, I=0.01 mol/L $NaNO_3$, T=293 K

where q_t (mg/g) represents the sorption capacity of Cd(II) at time t (h); k_1 (h^{-1}), k_2 (g/(mg·h)), k_i (g/(mg·h$^{1/2}$)) are the rate constants of 3 models, respectively; C (mg/L) indicates the thickness of boundary layer. The linear plots of 3 models went with Fig. 3(b-d), respectively. The corresponding parameters can be found in Table 1. We can see that the sorption kinetics could be fitted better by the pseudo-second-order kinetic model than pseudo-first-order kinetic model due to the higher correlation coefficients (R^2). The result implied the chemical sorption process[44]. More remarkable, all the sorption processes on MoS_2 at different pH contained 3 stages (Fig. 3(d)). The initial stage might be ascribed to Cd(II) ions diffusion from solution to the surface of MoS_2. Due to enough binding sites, high concentration Cd(II) ions and strong affinity between metal ions and S atoms[24-25], great numbers of Cd(II) were rapidly adsorbed onto the MoS_2 surface. The second stage is the intra-particle diffusion, which donated as Cd(II) intraparticle diffusion through 2D structure of MoS_2 with permeable channels[23]. The third stage on MoS_2 was the final equilibrium stage, which might be attributed to lack of binding sites or low concentration Cd(II) ions. Interestingly, the turning points in time at three stages were the same at solution pH 4.55, 5.34, 6.12. The intra-particle diffusion process mainly occurred after 1 h and the sorption reached equilibrium after 2 h. The sorption isotherms studies were carried out at different solution pH (*i.e.*, 4.55, 5.34, 6.12) and 3 temperatures (*i.e.*, 293, 313, 333 K), and the detailed results are shown in Fig. S2, Fig. S3 and Table S1, Table 2. The sorption isotherms were consistent with previous studies[45-48]. The thermodynamics implied that the sorption was a spontaneous, endothermic process[49-51].

2.3　EXAFS analysis

To reveal the interaction mechanisms between Cd(II) and MoS_2 at microscopic level, local structures of Cd(II) adsorbed on MoS_2 were investigated at various pH by EXAFS. The k^3-weighted, normalized, background-subtracted EXAFS spectra ($\sqrt{\chi}$-function) and the corresponding Fourier transformed radial structure functions (RSFs) magnitudes and imaginary parts of Cd(II) reference samples at 3 pH are shown in Fig. S4. The EXAFS oscillation of the $Cd(NO_3)_2$ (aq) was a single sinusoidal waveform arising from the backscattering of oxygen atoms in the first shell. The RSFs present similar characteristic and possess only one peak at ~0.2 nm. The existence of Cd–O bond and absence of direct binding for Cd(II) to MoS_2 surface imply a typical outer-sphere complexation of Cd(II)[36]. Cd(II) in $Cd(NO_3)_2$ (aq) was coordinated with 6.2 O atoms at interatom bond distance of 0.233 nm (Table S3), which differs from the study by Gräfe *et al.*[52]. Gräfe *et al.* found Cd was coordinated by 5.3 O atoms at the distance of 0.227 nm. The difference may attribute to the error of the EXAFS and XAFS methods. Unlike $Cd(NO_3)_2$ solution, the spectra and RSFs of $Cd(OH)_2$ precipitation were more complicated due to the presence of higher-shell atoms in the coordination environment of Cd(II). The first Cd–O distance was 0.238 nm coordinated with 6.1 O atoms and the second shell was simulated only with Cd–Cd contribution (R=0.359 nm, CN=5.9), which was close to the results from Gräfe *et al.* (Cd–O: R=0.229 nm, CN=6.7; Cd–Cd: R=0.353 nm, CN=5.6)[52]. The EXAFS spectra of the CdS compound show that Cd(II) can be directly bonded to MoS_2 surface by S atoms, hinting that an inner-sphere complexation occurs between Cd and S[53]. The single peak (0.24 nm) of RSFs shows the single shell of Cd–S (R=0.259 nm, CN=4.1). Fig. 4 shows that the EXAFS spectra and relevant RSFs of the sorption samples at different pH. Similarity of the spectra of the sorption samples at pH 3.56 and 6.48 to that of the CdS compound suggests that the microstructure of Cd adsorbed onto MoS_2 at low pH is similar to that of CdS complex and an inner-sphere complex forms at low pH. This inner-sphere complex is mainly present in 2D structure with large surface area and permeable channels of MoS_2 nanosheets. In addition, the spectrum at pH 9.57 is identical to that of $Cd(OH)_2$ precipitation. The peak of RSFs in second shell goes with Cd–Cd bonding, indicating the formation of $Cd(OH)_2$ precipitation at high pH. Totally, we found two sorption types: the inner-sphere complexation and the surface precipitation. The inner-sphere complexation mainly forms at lower pH which is similar to the microstructure of CdS compound. Thus Cd(II) could be directly adsorbed onto the surface of MoS_2 and then bind with S atoms (Fig. S5). The affinity

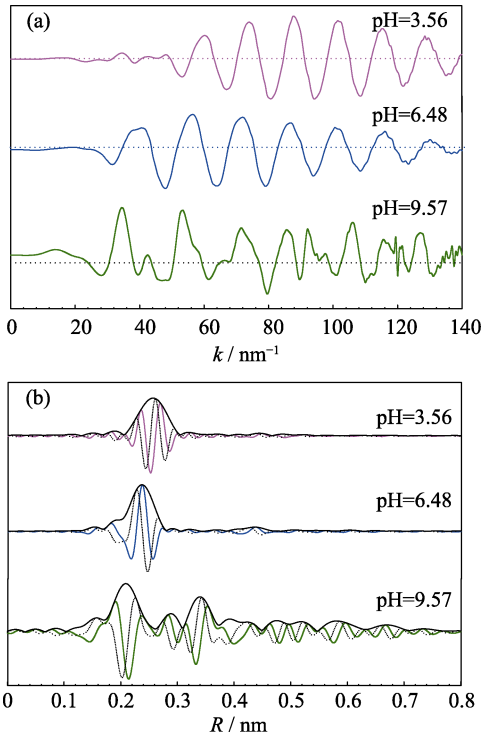

Fig. 4　Normalized, background-subtracted and k^3-weighted EXAFS spectra (a) and corresponding RSF magnitudes and imaginary parts (b) of Cd reference samples

of Cd–S bond is considered to be stronger than Cd–O bond, which determines the stability and excellent sorption capacity of MoS_2 as an adsorbent[21]. At higher pH, the $Cd(OH)_2$ precipitation is the main species, leading to immobility of Cd(II) onto MoS_2 surface. These interaction mechanisms and microstructure of Cd(II) and MoS_2 could explain macroscopic performance of the sorption at various pH and ionic strength.

3　Conclusions

In this work, the interaction mechanisms and microscopic structure of Cd(II) and MoS_2 nanosheets were investigated by batch experiments and EXAFS technology. In batch experiments, the pH-dependent and ionic strength-independent sorption of Cd(II) onto MoS_2 implied an inner-sphere complexation in the range of pH 3.3–9.6. The better fitted pseudo-second-order kinetics confirmed the chemical nature of the sorption and the intra-particle diffusion model reflected the sorption process from the surface to intra-particle diffusion to final equilibrium. The isotherms could be simulated better by Freundlich isotherms than by Langmuir isotherms model, indicating the heterogeneity of active sites on MoS_2. The thermodynamics implied the sorption at each pH was a spontaneous, endothermic, and irreversible process. The EXAFS spectra revealed the coexistence of two sorption types. The inner-sphere complexation was formed in the form of Cd–S bond

similar to CdS complex at pH 3.56 and 6.48, while the precipitation occurred in the form of Cd–O and Cd–Cd bonds similar to $Cd(OH)_2$ at pH 9.57. In summary, the interaction mechanisms and local structure of Cd(II) and MoS_2 are strongly affected by the solution pH.

Supporting materials

Supporting materials related to this article can be found at https://doi.org/10.15541/jim20190381.

References:

[1] ZENG G, LIU Y, TANG L, *et al.* Enhancement of Cd(II) adsorption by polyacrylic acid modified magnetic mesoporous carbon. *Chem. Eng. J.*, 2015, **259:** 153–160.

[2] YANG G, TANG L, LEI X, *et al.* Cd(II) removal from aqueous solution by adsorption on ketoglutaric acid-modified magnetic chitosan. *Appl. Surf. Sci.*, 2014, **292:** 710–716.

[3] LUO L, MA Y B, ZHANG S Z, *et al.* An inventory of trace element inputs to agricultural soils in China. *J. Environ. Manage*, 2009, **90(8):** 2524–2530.

[4] KHAN T A, CHAUDHRY S A, ALI I. Equilibrium uptake, isotherm and kinetic studies of Cd(II) adsorption onto iron oxide activated red mud from aqueous solution. *J. Mol. Liq.*, 2015, **202:** 165–175.

[5] AWUAL M R, KHRAISHEH M, ALHARTHI N H, *et al.* Efficient detection and adsorption of cadmium(II) ions using innovative nano-composite materials. *Chem. Eng. J.*, 2018, **343:** 118–127.

[6] LIAO Q, ZOU D, PAN W, *et al.* Highly-efficient scavenging of P(V), Cr(VI), Re(VII) anions onto g-C_3N_4 nanosheets from aqueous solutions as impacted *via* water chemistry. *J. Mol. Liq.*, 2018, **258:** 275–284.

[7] DONG L, YANG J, MOU Y, *et al.* Effect of various environmental factors on the adsorption of U(VI) onto biochar derived from rice straw. *J. Radioanal. Nucl. Chem.*, 2017, **314(1):** 377–386.

[8] SHENG G D, YANG Q, PENG F, *et al.* Determination of colloidal pyrolusite, Eu(III) and humic substance interaction: a combined batch and EXAFS approach. *Chem. Eng. J.*, 2014, **245:** 10–16.

[9] YU S J, WANG X X, PANG H W, *et al.* Boron nitride-based materials for the removal of pollutants from aqueous solutions: a review. *Chem. Eng. J.*, 2018, **333:** 343–360.

[10] YAO W, WANG X, LIANG Y, *et al.* Synthesis of novel flower-like layered double oxides/carbon dots nanocomposites for U(VI) and ^{241}Am(III) efficient removal: batch and EXAFS studies. *Chem. Eng. J.*, 2018, **332:** 775–786.

[11] WANG J, WANG X X, ZHAO G X, *et al.* Polyvinylpyrrolidone and polyacrylamide intercalated molybdenum disulfide as adsorbents for enhanced removal of chromium(VI) from aqueous solutions. *Chem. Eng. J.*, 2018, **334:** 569–578.

[12] LIAO Q, ZOU D S, PAN W, *et al.* Highly efficient capture of Eu(III), La(III), Nd(III), Th(IV) from aqueous solutions using g-C_3N_4 nanosheets. *J. Mol. Liq.*, 2018, **252:** 351–361.

[13] WANG X X, YU S J, WANG X K. Removal of radionuclides by metal-organic framework-based materials. *J. Inorg. Mater.*, 2019, **34(1):** 17–26.

[14] WANG N, PANG H, YU S, *et al.* Investigation of adsorption mechanism of layered double hydroxides and their composites on radioactive uranium: a review. *Acta Chim. Sinica*, 2019, **77(2):** 143–152.

[15] LIU X, MA R, WANG X, *et al.* Graphene oxide-based materials for efficient removal of heavy metal ions from aqueous solution: a review. *Environ. Pollut.*, 2019, **252:** 62–73.

[16] WANG X X, CHEN L, WANG L, *et al.* Synthesis of novel nanomaterials and their application in efficient removal of radionuclides. *Sci. China Chem.*, 2019, **62(8):** 933–967.

[17] FENG B, YAO C, CHEN S, *et al.* Highly efficient and selective recovery of Au(III) from a complex system by molybdenum disulfide nanoflakes. *Chem. Eng. J.*, 2018, **350:** 692–702.

[18] CHEN H J, HUANG J, LEI X L, *et al.* Adsorption and diffusion of lithium on MoS_2 monolayer: the role of strain and concentration. *Int. J. Electrochem. Sci.*, 2013, **8:** 2196–2203.

[19] JIA F, WANG Q, WU J, *et al.* Two-dimensional molybdenum disulfide as a superb adsorbent for removing Hg^+ from water. *ACS Sustainable Chem. Eng.*, 2017, **5:** 7410–7419.

[20] JIA F, ZHANG X, SONG S. AFM study on the adsorption of Hg^{2+} on natural molybdenum disulfide in aqueous solutions. *Phys. Chem. Chem. Phys.*, 2017, **19:** 3837−3844.

[21] WANG Z, MI B. Environmental applications of 2D molybdenum disulfide (MoS_2) nanosheet. *Environ. Sci. Technol.*, 2017, **51:** 8229–8244.

[22] AI K, RUAN C, SHEN M, *et al.* MoS_2 nanosheets with widened interlayer spacing for high-efficiency removal of mercury in aquatic systems. *Adv. Funct. Mater.*, 2016, **26:** 5542–5549.

[23] TONG S, DENG H, WANG L, *et al.* Multi-functional nanohybrid of ultrathin molybdenum disulfide nanosheets decorated with cerium oxide nanoparticles for preferential uptake of lead (II) ions. *Chem. Eng. J.*, 2018, **335:** 22–31.

[24] LI X, LI Q, LINGHU W, *et al.* Sorption properties of U(VI) and Th(IV) on two-dimensional molybdenum disulfide (MoS_2) nanosheets: effects of pH, ionic strength, contact time, humic acids and temperature. *Environ. Technol. Innov.*, 2018, **11:** 328–338.

[25] WANG Q, YANG L, JIA F, *et al.* Removal of Cd(II) from water by using nano-scale molybdenum disulphide sheets as adsorbents. *J. Mol. Liq.*, 2018, **263:** 526–533.

[26] ZHI L, ZUO W, CHEN F, *et al.* 3D MoS_2 composition aerogel as chemosensors and adsorbents for colorimetric detection and high-capacity adsorption of Hg^{2+}. *ACS Sustain. Chem. Eng.*, 2016, **4:** 3398−3408.

[27] AI K, RUAN C, SHEN M, *et al.* MoS_2 nanosheets with widened interlayer spacing for high-efficiency removal of mercury in aquatic systems. *Adv. Funct. Mater.*, 2016, **26:** 5542−5549.

[28] AGHAGOLI M J, BEYKI M H, SHEMIRANI F. Application of dahlia-like molybdenum disulfide nanosheets for solid phase extraction of Co(II) in vegetable and water samples. *Food Chem.*, 2017, **223:** 8−15.

[29] GAO X, SHENG G D, HUANG Y Y. Mechanism and microstructure of Eu(III) interaction with γ-MnOOH by a combination of batch and high resolution EXAFS investigation. *Sci. China Chem.*, 2013, **56:** 1658–1666.

[30] DONG L, LIAO Q, LINGHU W, *et al.* Application of EXAFS with a bent crystal analyzer to study the pH-dependent microstructure of Eu(III) onto birnessite. *J. Environ. Chem. Eng.*, 2018, **6:** 842–848.

[31] VASCONCELOS I F, HAACK E A, MAURICE P A, *et al.* EXAFS analysis of cadmium(II) adsorption to kaolinite. *Chem. Geol.*, 2008,

249: 237–249.

[32] LIU C, FRENKEL A I, VAIRAVAMURTHY A, *et al.* Sorption of cadmium on humic acid: mechanistic and kinetic studies with atomic force microscopy and X-ray absorption fine structure spectroscopy. *Can. J. Soil Sci.*, 2001, **81:** 337–348.

[33] SHENG G D, YANG S T, LI Y M, *et al.* Retention mechanisms and microstructure of Eu(III) on manganese dioxides studied by batch and high resolution EXAFS technique. *Radiochim. Acta*, 2014, **102:** 155–167.

[34] COLEMAN J N, LOTYA M, O'NEILL A, *et al.* Two dimensional nanosheets produced by liquid exfoliation of layered materials. *Science*, 2011, **331(6017):** 568−571.

[35] SPLENDIANI A, SUN L, ZHANG Y, *et al.* Emerging photoluminescence in monolayer MoS_2. *Nano Lett.*, 2010, **10:** 1271−1275.

[36] KUMAR A S K, JIANG S J, WARCHOL J K. Synthesis and characterization of two-dimensional transition metal dichalcogenide magnetic MoS_2@Fe_3O_4 nanoparticles for adsorption of Cr(VI)/Cr(III). *ACS Omega*, 2017, **2:** 6187–6200.

[37] TAKAMATSU R, ASAKURA K, CHUN W J, *et al.* EXAFS studies about the sorption of cadmium ions on montmorillonite. *Chem. Lett.*, 2006, **35:** 224–225.

[38] HUANG X, CHEN T, ZOU X, *et al.* The adsorption of Cd(II) on manganese oxide investigated by batch and modeling techniques. *Int. J. Environ. Res. Public Health*, 2017, **14(10):** 1145.

[39] GUECHI E, BEGGAS D. Removal of cadmium (II) from water using fibre fruit lufa as biosorbent. *Desalin. Water Treat.*, 2017, **94:** 181–188.

[40] ABASIYAN S M A, MAHDANINIA G R. Polyvinyl alcohol-based nanocomposite hydrogels containing magnetic laponite RD to remove cadmium. *Environ. Sci. Poll. Res.*, 2018, **25:** 14977–14988.

[41] CORBETT J F. Pseudo first-order kinetics. *J. Chem. Educ.*, 1972, **49:** 663.

[42] HO Y S, MCKAY G. A comparison of chemisorption kinetic models applied to pollutant removal on various sorbents. *Process. Saf. Environ.*, 1998, **76:** 332–340.

[43] GRAAF G H, SCHOLTENS H, STAMHUIS E J, *et al.* Intra-particle diffusion limitations in low-pressure methanol synthesis. *Chem. Eng. Sci.*, 1990, **45:** 773–783.

[44] HO Y S, MCKAY G. The kinetics of sorption of divalent metal ions onto sphagnum moss peat. *Water Rer.*, 2000, **34:** 735–742.

[45] TEMKIN M J, PYZHEV V. Recent modifications to Langmuir isotherms. *Acta Physchim*, 1940, **12:** 217–222.

[46] XUE C, QI P S, LIU Y Z. Adsorption of aquatic Cd^{2+} using a combination of bacteria and modified carbon fiber. *Adsorpt. Sci. Technol.*, 2017, **36:** 857–871.

[47] GU P, ZHANG S, ZHANG C, *et al.* Two-dimensional MAX-derived titanate nanostructures for efficient removal of Pb(II). *Dalton Trans.*, 2019, **48(6):** 2100–2107.

[48] CHEN W, LU Z, XIAO B, *et al.* Enhanced removal of lead ions from aqueous solution by iron oxide nanomaterials with cobalt and nickel doping. *J. Clean. Prod.*, 2019, **211:** 1250–1258.

[49] ZHANG D, NIU H Y, ZHANG X L, *et al.* Strong adsorption of chlorotetracycline on magnetite nanoparticles. *J. Hazard. Mater.*, 2011, **192:** 1088–1093.

[50] ZHANG H, YU X, CHEN L, *et al.* Study of ^{63}Ni adsorption on NKF-6 zeolite. *J. Environ. Radioact.*, 2010, **101:** 1061–1069.

[51] BEKCI Z, SEKI Y, YURDAKOC M K. A study of equilibrium and FTIR, SEM/EDS analysis of trimethoprim adsorption onto K10. *J. Mol. Struct.*, 2007, **827:** 67–74.

[52] GRÄFE M, SINGH B, BALASUBRAMANIAN M. Surface speciation of Cd(II) and Pb(II) on kaolinite by EXAFS spectroscopy. *J. Colloid Interf. Sci.*, 2007, **315:** 21–32.

[53] SHENG G, DONG H, SHEN R, *et al.* Microscopic insights into the temperature dependent adsorption of Eu(III) onto titanate nanotubes studied by FTIR, XPS, XAFS and batch technique. *Chem. Eng. J.*, 2013, **217:** 486–494.

不同 pH 条件下硫化钼纳米片吸附 Cd(II)的微观机制研究

董丽佳[1], 郭筱洁[2], 李 雪[1], 陈朝贵[1], 金 阳[1], AHMED Alsaedi[3], TASAWAr Hayat[3,4], 赵轻舟[5], 盛国栋[6]

(1. 绍兴文理学院 生命科学院, 绍兴 312000; 2. 杭州电子大学 材料与环境工程学院, 杭州 310018; 3. NAAM Research Group, Department of Mathematics, Faculty of Science, King Abdulaziz University, Jeddah 21589, Sudi Arabia; 4. Department of Mathematics, Quaid-I-Azam University, Islamabad 44000, Pakistan; 5. 中国科学院大学 资源与环境学院, 北京 100049; 6. 绍兴文理学院 化学与化工学院, 绍兴 312000)

摘 要: 本研究结合静态实验和 X 射线吸收精细结构谱学(EXAFS)评估了硫化钼纳米片对重金属 Cd(II)的吸附行为和微观机制。结果表明: Cd(II)在硫化钼纳米片上的吸附受溶液 pH、反应时间和温度的显著影响, 但不受离子强度的影响。在 pH 3.3~9.6 范围内, pH 升高显著促进了硫化钼对 Cd(II)的吸附量, 但不改变吸收速率、吸附等温线和热力学。二级动力学模型能更好地拟合该吸附平衡, 且内表面颗粒扩散模型显示了吸附过程中的三个典型阶段。等温线和热力学分析说明 Cd(II)在硫化钼上的吸附是异质性的、自发的、吸热的和不可逆的过程。EXAFS 光谱学分析揭示了该吸附存在两种类型: 在较低的 pH(3.56, 6.48)条件下, 内表面络合以 Cd–S 配位键为主; 在较高的 pH(9.57)条件下, 出现 $Cd(OH)_2$ 沉淀, 且配位键以 Cd–O 和 Cd–Cd 的形式存在。这些研究结果对于评估重金属离子和硫化钼纳米片在分子水平上的作用机理提供了新的视野。

关 键 词: 硫化钼纳米片; pH; 微观结构; EXAFS; Cd(II)

中图分类号: TQ174 **文献标识码:** A

Supporting Materials

Microscopic Insights into pH-dependent Adsorption of Cd(II) on Molybdenum Disulfide Nanosheets

DONG Lijia[1], GUO Xiaojie[2], LI Xue[1], CHEN Chaogui[1], JIN Yang[1], AHMED Alsaedi[3], TASAWAR Hayat[3,4], ZHAO Qingzhou[5], SHENG Guodong[6]

(1. School of Life Science, Shaoxing University, Shaoxing 312000, China; 2. College of Materials & Environmental Engineering, Hangzhou Dianzi University, Hangzhou 310018, China; 3. NAAM Research Group, Department of Mathematics, Faculty of Science, King Abdulaziz University, Jeddah 21589, Saudi Arabia; 4. Department of Mathematics, Quaid-I-Azam University, Islamabad 44000, Pakistan; 5. College of Resources and Environment, University of Chinese Academy of Sciences, Beijing 100049, China; 6. College of Chemistry and Chemical Engineering, Shaoxing University, Shaoxing 312000, China)

Characterization of MoS_2 nanosheets

The morphologies and microstructures of MoS_2 nanosheets were characterized by SEM, TEM, XRD, FT-IR, Zeta potentials, AFM, and EDX. Both SEM and TEM images (Fig. S1(a,b)) show the obvious 2D layered structure of MoS_2 and its typical diameter ranges from hundreds of nanometers to several micrometers, implying ultrathin nature[1-3]. The peak number of XRD (Fig. S1(c)) implies relatively high purity of MoS_2. The visible dominant peak (2θ=~17°) confirms the nature of MoS_2 nanosheets and the well-stacked crystalline structure[4]. The FT-IR spectrum (Fig. S1(d)) indicates functional groups on MoS_2. The peak at ~3550 cm^{-1} arises from the stretching vibration of –OH groups. The peaks at ~1700 and ~1400 cm^{-1} match with the C=O stretching vibration and O–H deformation vibration, respectively[5]. The peak at ~600 cm^{-1} is attributed to the bend vibration of MoS_2 water. The Zeta potential (Fig. S1(e)) suggests that the zero charge (pH_{pzc}) point of MoS_2 samples be ~3.93. AFM

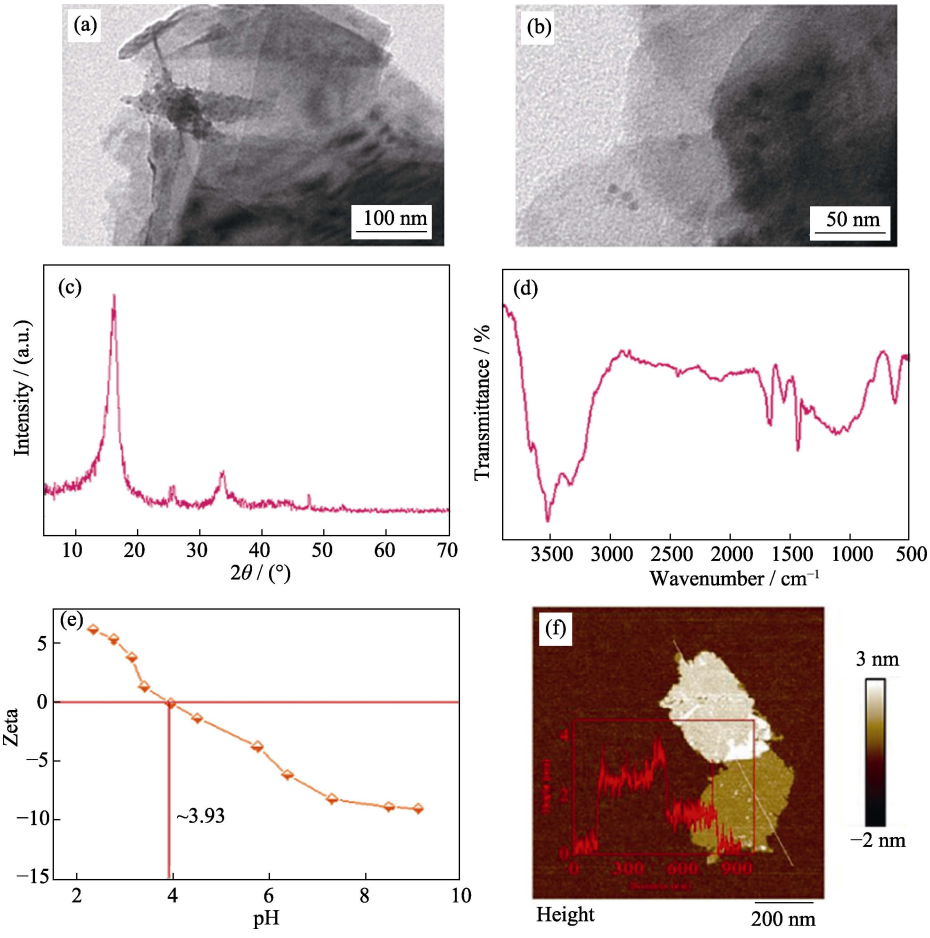

Fig. S1　SEM image (a), TEM image (b), XRD pattern (c), FT-IR spectrum (d), Zeta potentials (e), and height cross-section profile (inset) and corresponding AFM image (f) of MoS_2 samples

image illustrates that most MoS_2 nanosheets are thin. The height (~2.0 nm) of the cross-section implies the presence of a few layers of MoS_2 nanosheets (Fig. S1(f)).

Sorption isotherms and thermodynamics

The sorption isotherms studies were carried out at different pH (*i.e.*, 4.55, 5.34, 6.12) and 3 temperatures (*i.e.*, 293, 313, 333 K) (Fig. S2). In Fig. S2(a), the sorption amount of Cd(II) on MoS_2 was promoted by high temperature at each solution pH and also by high pH at each temperature, implying that pH had no impact on temperature effects. All equilibrium data were modeled using the linear forms of Langmuir and Freundlich isotherms by the following equations[6]:

$$\frac{C_e}{q_e}=\frac{1}{K_L q_{max}}+\frac{C_e}{q_{max}} \quad (S1)$$

$$\lg q_e=\lg k_F+n\lg C_e \quad (S2)$$

where q_{max} (mg/g) and K_L (L/mg) are the maximum sorption capacity of Cd(II) on per weight unit of MoS_2 and the Langmuir affinity parameter, respectively; n and K_F ($mg^{1-n}\cdot L^n/g$) represent the exponent and Freundlich affinity-capacity parameter, respectively. Combined the linear plots of fitted isotherms (Fig. S2(b,c)) with the corresponding isotherm parameters (Table S2), it was concluded that the sorption processes at each pH were more appropriately fitted by Freundlich model than Langmuir model due to higher R^2 values, which was consistent with previous studies[7-9]. This result could be attributed to the heterogeneity distribution of active sites on MoS_2 surface determined by the anisotropic structure of MoS_2. Thereby, the sorption behavior of Cd(II) on MoS_2 was greatly determined by the special structure of interior sulfur atoms. The thermodynamic parameters, the Gibbs free energy (ΔG^θ), the enthalpy (ΔH^θ), and the entropy (ΔS^θ), were calculated as follows:

$$\Delta G^\theta=-RT\ln K^\theta \quad (S3)$$

$$\ln K^\theta=\Delta S^\theta/R-\Delta H^\theta/RT \quad (S4)$$

where K^θ is the distribution coefficient, and the values of $\ln K^\theta$ at each pH are assessed by plotting $\ln K_d$ *vs.* C_e (Fig. S3(a)). The ΔS^θ at each pH is calculated from the slope of linear plot of ΔG^θ *vs.* T (Fig. S3(b)). The correlated thermodynamic parameters are recorded in Table S3. It can be inferred that Cd(II) sorption on MoS_2 at each solution pH was a spontaneous, endothermic, and irreversible process due to $\Delta G^\theta<0$, $\Delta H^\theta>0$, and $\Delta S^\theta>0$[10]. More negative values of ΔG^θ proved the enhancement of the high temperature on the sorption. In addition, the sizes of ΔG^θ and ΔH^θ revealed chemical nature and existence of physical forces[11-12].

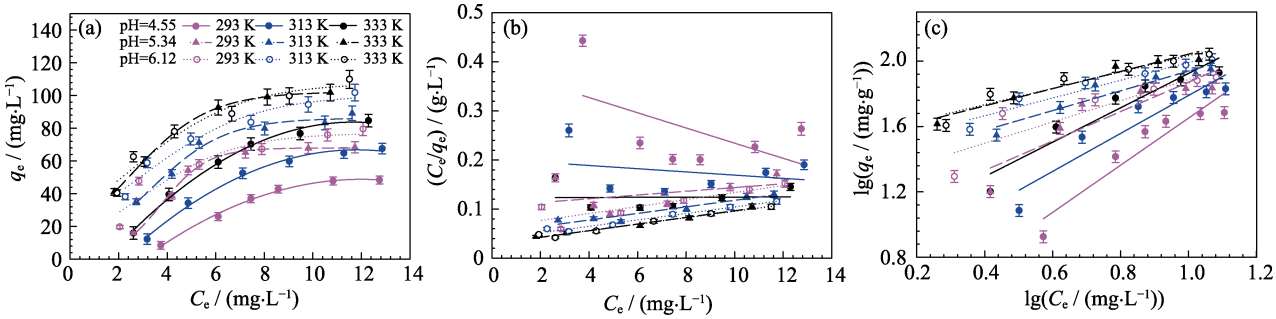

Fig. S2 Adsorption isotherms (a) and fitting results of Langmuir (b) and Freundlich (c) sorption isotherms of Cd(II) sorption on MoS_2 at different temperatures and different pH

Cd(II) initial concentration=10 mg/L, m/V=0.15 g/L, I = 0.01 mol/L $NaNO_3$

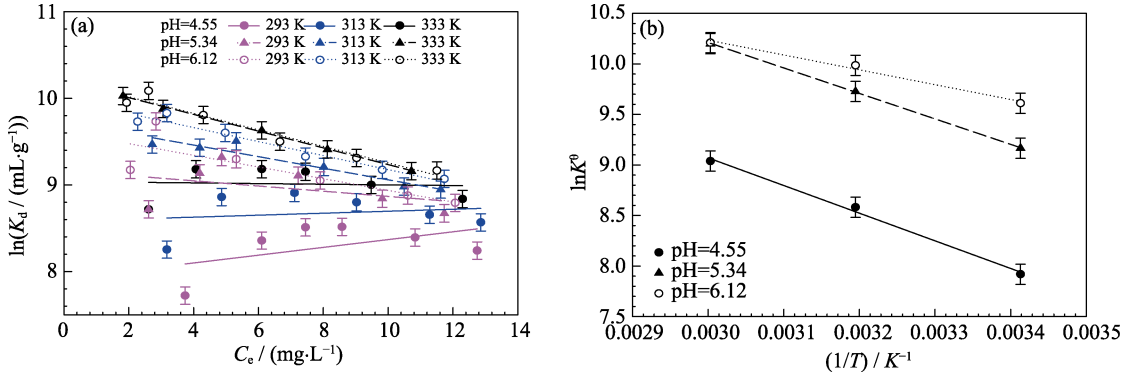

Fig. S3 Linear plots of $\ln K_d$ *versus* C_e for Cd(II) at different temperatures and different pH(a), and linear regression plots of $\ln K^\theta$ *versus* $1/T$ for Cd(II) sorption on MoS_2 at different pH(b)

Cd(II) initial concentration=10 mg/L, m/V=0.15 g/L, I=0.01 mol/L $NaNO_3$

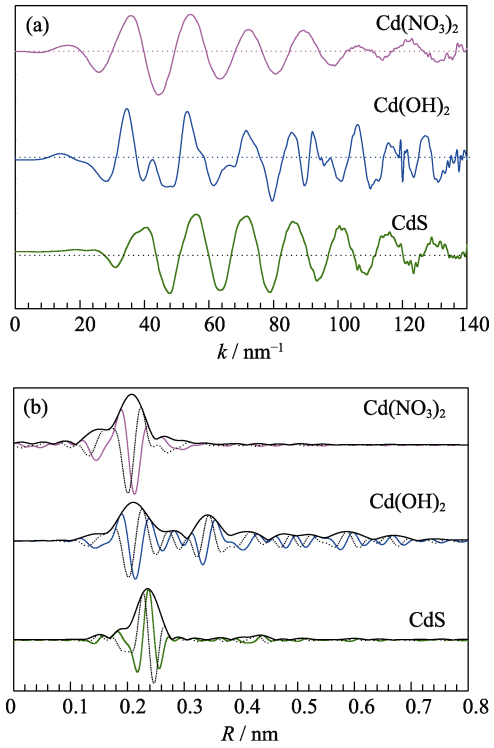

Fig. S4　EXAFS spectra (a) and the corresponding RSF magnitudes and imaginary parts (b) of Cd reference samples

Table S1　Parameters of Langmuir and Freundlich equations for the sorption of Cd(II) onto MoS_2 at different temperatures and different pH

(Cd(II) initial concentration=10 mg/L, m/V=0.15 g/L, I=0.01 mol/L $NaNO_3$)

	pH	T/K	K_F/(mg^{1-n}·L^n·g^{-1})	n	R^2
Freundlich equation	4.55	293	1.624	1.440	0.887
		313	4.256	1.160	0.881
		333	7.461	1.052	0.904
	5.34	293	9.363	0.899	0.801
		313	21.627	0.603	0.907
		333	32.734	0.526	0.939
	6.12	293	17.298	0.650	0.812
		313	28.054	0.542	0.935
		333	34.119	0.499	0.919
	pH	T/K	q_{max}/(mg·g^{-1})	K_L/(L·mg^{-1})	R^2
Langmuir equation	4.55	293	0.040	64.516	0.299
		313	0.016	305.157	0.069
		333	0.001	754.717	0.017
	5.34	293	0.036	262.536	0.162
		313	0.132	149.276	0.918
		333	0.236	147.580	0.978
	6.12	293	0.114	140.449	0.759
		313	0.172	152.022	0.974
		333	0.224	151.492	0.978

Table S2　Parameters of thermodynamics for adsorption of Cd(II) onto MoS_2 at 3 temperatures and different pH

(Cd(II) initial concentration=10 mg/L, m/V=0.15 g/L, I = 0.01 mol/L $NaNO_3$)

pH	T	ΔG^θ/(kJ/mg)	ΔS^θ/(J·mg^{-1}· K^{-1})	ΔH^θ/(kJ·mg^{-1})
4.55	293	–19.291	143.66592	22.803
	313	–22.333		22.635
	333	–25.022		22.818
5.34	293	–22.331	147.73978	20.957
	313	–25.312		20.930
	333	–28.239		20.958
6.12	293	–23.412	121.71696	12.251
	313	–25.986		12.111
	333	–28.267		12.265

Table S3　Structural parameters of Cd(II) reference and sorption samples

Sample conditions	shells	R/nm	CN	σ^2 /nm^2
$Cd(NO_3)_2$(aq)	Cd–O	0.233(4)	6.2(3)	0.0010(1)
$Cd(OH)_2$	Cd–O	0.238(2)	6.1(4)	0.0014(5)
	Cd–Cd	0.359(3)	5.9(4)	0.0032(5)
CdS	Cd–S	0.259(1)	4.1(3)	0.0024(2)
pH 3.56, sorption	Cd–S	0.255(2)	3.9(5)	0.0027(3)
pH 6.48, sorption	Cd-S	0.257(1)	3.8(4)	0.0023(5)
pH 9.57, sorption	Cd-O	0..34(5)	5.9(6)	0.0016(3)
	Cd-Cd	0.357(3)	5.6(4)	0.0037(2)

R-Bond distance, CN-Coordination number, σ^2-Debye-Waller factor

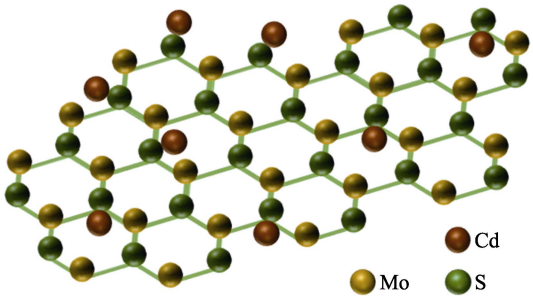

Fig. S5　Schematic representation of possible sorption sites on the surface of MoS_2

References:

[1] WANG Q, YANG L, JIA F, *et al.* Removal of Cd(II) from water by using nano-scale molybdenum disulphide sheets as adsorbents. *J. Mol. Liq*., 2018, **263:** 526–533.

[2] COLEMAN J N, LOTYA M, O'NEILL A, *et al.* Two dimensional nanosheets produced by liquid exfoliation of layered materials. *Science*, 2011, **331:** 568−571.

[3] SPLENDIANI A, SUN L, ZHANG Y, *et al.* Emerging photoluminescence in monolayer MoS_2. *Nano Lett*., 2010, **10:** 1271−1275.

[4] KUMAR A S K, JIANG S J, WARCHOL J K. Synthesis and characterization of two-dimensional transition metal dichalcogenide magnetic MoS_2@Fe_3O_4 nanoparticles for adsorption of Cr(VI)/Cr(III). *ACS Omega*, 2017, **2:** 6187–6200.

[5] TONG S, DENG H, WANG L, *et al.* Multi-functional nanohybrid

of ultrathin molybdenum disulfide nanosheets decorated with cerium oxide nanoparticles for preferential uptake of lead (II) ions. *Chem. Eng. J*., 2018, **335:** 22–31.

[6] TEMKIN M J, PYZHEV V. Recent modifications to langmuir isotherms. *Acta Physchim*., 1940, **12:** 217–222.

[7] XUE C, QI P S, LIU Y Z. Adsorption of aquatic Cd^{2+} using a combination of bacteria and modified carbon fiber. *Adsorpt. Sci. Technol*., 2017, **36:** 857–871.

[8] GU P, ZHANG S, ZHANG C, *et al*. Two-dimensional MAX-derived titanate nanostructures for efficient removal of Pb(II). *Dalton Trans*., 2019, **48(6):** 2100–2107.

[9] CHEN W, LU Z, XIAO B, *et al*. Enhanced removal of lead ions from aqueous solution by iron oxide nanomaterials with cobalt and nickel doping. *J. Clean. Prod*., 2019, **211:** 1250–1258.

[10] ZHANG D, NIU H Y, ZHANG X L, *et al.* Strong adsorption of chlorotetracycline on magnetite nanoparticles. *J. Hazard. Mater*., 2011, **192:** 1088–1093.

[11] ZHANG H, YU X, CHEN L, *et al.* Study of ^{63}Ni adsorption on NKF-6 zeolite. *J. Environ. Radioact*., 2010, **101:** 1061–1069.

[12] BEKCI Z, SEKI Y, YURDAKOC M K. A study of equilibrium and FTIR, SEM/EDS analysis of trimethoprim adsorption onto K10. *J. Mol. Struct*., 2007, **827:** 67–74.